HHS Public Access

Author manuscript

Nat Methods. Author manuscript; available in PMC 2017 January 18.

Published in final edited form as:

Nat Methods. 2016 September ; 13(9): 755–758. doi:10.1038/nmeth.3926.

LOVTRAP, An Optogenetic System for Photo-induced Protein Dissociation

Hui Wang[1,9], **Marco Vilela**[2,9], **Andreas Winkler**[3,4], **Miroslaw Tarnawski**[3], **Ilme Schlichting**[3], **Hayretin Yumerefendi**[5], **Brian Kuhlman**[5], **Rihe Liu**[6,7], **Gaudenz Danuser**[2], and **Klaus M Hahn**[1,8]

[1]Department of Pharmacology, University of North Carolina Chapel Hill, Chapel Hill, NC, U.S.A

[2]Lyda Hill Department of Bioinformatics, UT Southwestern Medical Center, Dallas, TX, U.S.A

[3]Department of Biomolecular Mechanisms, Max Planck Institute for Medical Research, Heidelberg, Germany

[5]Department of Biochemistry and Biophysics, University of North Carolina Chapel Hill, Chapel Hill, NC,, U.S.A

[6]Eshelman School of Pharmacy, University of North Carolina Chapel Hill, Chapel Hill, NC, U.S.A

[7]Carolina Center for Genome Sciences, University of North Carolina Chapel Hill, Chapel Hill, NC, U.S.A

[8]Lineberger Cancer Center, University of North Carolina Chapel Hill, Chapel Hill, NC, U.S.A

Abstract

Here we introduce LOVTRAP, an optogenetic approach for reversible, light-induced protein dissociation. LOVTRAP is based on protein A fragments that bind to the LOV domain only in the dark, with tunable kinetics and a >150-fold change in K_d. By reversibly sequestering proteins at mitochondria, we precisely modulated the proteins' access to the cell edge, demonstrating a naturally occurring 3 mHz cell edge oscillation driven by interactions of Vav2, Rac1 and PI3K.

Direct correspondence to K.M.H. (khahn@med.unc.edu), G. D. (Gaudenz.Danuser@UTSouthwestern.edu), and R. L. (rliu@email.unc.edu).

[4]Current address: Institute of Biochemistry, Graz University of Technology,, Graz, Austria

[9]These authors contributed equally to this work.

ACCESSION CODES:

Atomic coordinates and structure factors have been deposited in the Protein Data Bank under accession codes: 5EFW (LOV2-Zdk1 complex), 5DJT (LOV2-Zdk2 complex), 5DJU (LOV2-Zdk3 complex).

AUTHOR CONTRIBUTIONS

H.W. performed the screening experiments, engineered proteins and performed imaging studies. M.V. performed analysis of oscillating signaling behavior. A.W., M.T. and I.S. carried out crystallography. H.W., H.Y. and B.K. purified proteins for crystallography. R.L., G.D. and K.M.H. directed the work and final edited the paper, which was written using contributions from all authors.

COMPETING FINACIAL INTERESTS STATEMENT

The authors declare no competing financial interests.

The ability to control proteins with light has been extended beyond engineering light-controlled ion channels, to activatation of non-channel proteins through fusion with light-sensitive plant proteins[1]. This has revealed important roles for transient subcellular localization and activation kinetics in signaling[1]. Here we describe LOVTRAP (LOV2 Trap and Release of Protein), an optogenetic approach capable of repeatedly and reversibly controlling protein activity with precise kinetics, and applicable to different proteins. The approach is based upon a small protein, which we named Zdark (Zdk), generated by mRNA display screening of a library derived from the Z subunit of protein A. Zdk binds selectively to the dark state of LOV2, a photo-sensor domain from *Avena sativa* phototropin 1. We anchored either Zdk or LOV2 away from the site where the protein of interest (POI) acted, and fused the POI to the non-anchored member of the pair (Fig. 1a). In the dark the POI was sequestered away from its site of action; upon irradiation, Zdk dissociated from LOV2, freeing the POI to move to its site of action. This approach improves upon previously available methods in several ways: important to the biological proof-of-principal studies described here, it provides diffusion limited activation kinetics (proteins are released in less than a second) and deactivation rates can be tuned from seconds to minutes using mutations described below. The approach is broadly applicable, as the POI simply needs to be fused to either LOV or Zdk. The method reduces 'leakiness', or dark state background activity: Anchored LOV2 can be expressed in excess of the POI, so that even if a small equilibrium amount of LOV2 is in the "lit"/nonbinding conformation in the dark, there is still sufficient anchored LOV2 to sequester the POI (Supplementary Note, Supplementary Fig. 1). Finally, proteins are not controlled through light-induced delivery to specific subcellular locations; hence they can act at multiple localizations upon activation.

Zdk was generated using a library based on the Z domain of immunoglobulin binding staphylococcal protein A[2]. The Z domain is a small, tightly folded three helix bundle. It contains no cysteines or disulfides that could be reduced and contribute to unfolding in cells. Thirteen residues along the first and second helices were randomized using an NNK codon[2] (Fig. 1b) to generate an mRNA-displayed protein library containing 5×10^{13} unique Z variants. After 12 rounds of selection, the enriched cDNA library was sequenced and the binding of 20 candidates with two consensus sequences were analyzed. Fig. 1c shows the binding properties of the three Zdk variants selected for further use. A radiometric binding assay showed that Zdk1, the candidate with the greatest difference in affinity for LOV's lit versus dark states, had 26.2 nM affinity for a LOV2 mutant fixed in the dark state (C450A[3]), but $K_d > 4$ μM for a lit state mutant (I539E[4]) (Fig. 1c). A model based on this affinity showed that caging was optimal when the mitochondrial anchor was expressed at 5–10 fold excess over the other component (Fig. 1d). The crystal structure of LOV2 complexed with Zdk1 showed that LOV2's C-terminal helix Jα, which unwinds upon irradiation[5], was inserted into a pocket formed by the first two helices of Zdk1 (Fig. 1e, Supplementary Figs. 2 & 3, Supplementary Table 1, Movie 1). Consistent with this crystal structure, mutations near the LOV2 C-terminus abolished binding, while mutations on other portions of the Jα helix had no effect (Supplementary Fig. 3). Zdk2 and Zdk3 showed smaller differences in lit/dark affinity (Fig. 1c), and their binding did not require interaction with the LOV C-terminal helix (Supplementary Figs. 2 & 4, Supplementary Table 1). Zdk2 and Zdk3 will be useful in applications in which proteins must be appended to the LOV C-terminus.

To examine the kinetics of protein activation and inactivation using LOVTRAP in living cells, the N-terminus of LOV2 was fused to mCherry fluorescent protein, and the N-terminus of Zdk was fused to a fragment of TOM20, a mitochondrial anchoring sequence[6]. When the two proteins were co-expressed in HeLa cells, mCherry was localized at mitochondria in the dark, but generated diffuse cytoplasmic distribution within 1 second after irradiation with 450–490 nm light (Fig. 2a, Supplementary Fig. 4, Movie 2). Cycling between the lit and dark distributions at least 10 times showed no diminution of the release or return to the mitochondria (Fig. 2b). Use of LOV mutants incapable of undergoing light-induced conformational changes showed only mitochondrial localization even after prolonged irradiation (Supplementary Fig. 5, Movie 3). Using wild type LOV2, the half-life for return of diffuse mCherry to the mitochondria was 18.5 seconds (Fig. 2c). These kinetics were tunable, using known and novel mutations of the LOV2 domain (Supplementary Table 2)[7, 8], enabling us to vary the $t_{1/2}$ of return from 1.7 to 496 seconds (Fig 2c). Fast rates are useful to control signaling with precise kinetics, while slow kinetics enable continuous activation with minimal irradiation (eg for the V416L mutant, a 1 second light pulse every 2.5 minutes will maintain greater than 80% activity). Finally we tested the ability of LOVTRAP to reversibly anchor the POI at points other than mitochondria; fusion of Zdk with an N-terminal fragment of Lyn kinase[9] led to reversible translocation of LOV2 between the cytosol and plasma membrane (Fig. 2d, Movie 4).

Regulatory processes controlling cell edge protrusion and retraction are driven by feedback interactions among signaling proteins[10, 11]. At steady state, the cell edge oscillates on a time scale of 1 – 5 minutes[12]. We leveraged the kinetic control of LOVTRAP to mimic the activation and deactivation of signals that drive these oscillations, focusing on the GTPases Rac1 and RhoA, and their upstream GTP exchange factor Vav2. In order to control these proteins' activity without influence from endogenous regulatory pathways, we fused Zdk to constitutively active mutants of RhoA (Q63L) and Rac1 (Q61L), and to a constitutively active fragment of Vav2 (aa 185-575[13], Supplementary Table 3). In HeLa cells, release of each protein (henceforth referred to as protein "activation") produced different effects on edge velocity, ruffling, cell area and protrusion distribution (Fig. 2e, f, g, h, i, and j, Supplementary Figs. 6, Movie 5, 6 and 7). Before irradiation, expression of LOVTRAP Vav2, LOVTRAP Rac1 and LOVTRAP RhoA had little effect on endogenous Rac1 expression, cell edge protrusion or mitochondrial function (Supplementary Figs. 8,9,10 and 11).

To further analyze the protrusion and retraction events induced by activation of Vav2, Rac1 and RhoA we turned to morphodynamic profiling[12], in which the cell edge was tracked before, during, and after optogenetic stimulation (Movie 8) and quantified the behavior in an edge velocity kymograph, where each row represents the velocity evolution of a particular location on the cell edge over time (Fig. 3a). Strikingly, activation of Vav2 did not just induce a spike of positive velocity, but instead generated a sustained increase in protrusion and retraction velocities. This suggested that an elevated state of Vav2 signaling contributes to both protrusion and retraction responses.

We suspected that frequency spectra of protrusion/retraction cycles would undergo changes during Vav2 activation and deactivation, as elevated Vav2 activity would gradually turn on

different downstream effector pathways with different response kinetics. We therefore implemented the Hilbert-Huang transform[14] to define for each location along the cell edge an instantaneous frequency density spectrum (see Methods, Supplementary Fig. 12). Spectra from all locations were integrated into a per-cell spectrogram (Fig. 3b, left), and temporally averaged for the periods before, during, and after Vav2 activation (Fig. 3b, right). Before and after activation the spectra displayed a uni-modal distribution with a peak at ~0.5 mHz, corresponding approximately to the inverse of the 1800 sec long time window of observation. Upon Vav2 activation, a peak emerged at 2.9 mHz, reflecting a global stimulation of protrusion-retraction-protrusion cycles of ~330 sec duration. Owing to the regularity of this response across a cell population we hypothesized that ~3 mHz reflected the principal frequency of a resonator.

To test this we exploited the kinetic control and rapid reversibility of LOVTRAP-Vav2 to optogenetically entrain oscillatory cycles. Indeed, we found that pulses of blue light of 50 s ‘on’ and 250 s ‘off’ generated highly synchronized protrusion-retraction cycles with a 3.3 mHz frequency (Fig. 3c and Supplementary Fig. 13a). Further support for the resonator hypothesis came from the observation that cycles could not be entrained when exposing LOVTRAP-Vav2 to pulses of 50 s ‘on’ and 200 s ‘off’ (4 mHz), whereas pulses of 6.7 mHz and 10.0 mHz, i.e. multiples of the putative principal resonator frequency, did entrain cycles, but again at 3.3 mHz (Fig. 3c and Supplementary Fig. 13b). Of note, in all experiments we observed several peaks at frequencies below 3.3 mHz. These may be the product of secondary resonating circuits or represent lower harmonics of the primary resonator, such as the peaks at 1.1 mHz.

Our data suggested Vav2 is part of an activator circuitry that stimulates protrusion, most probably through its role as an activating GEF of Rac1 GTPase, which drives actin filament assembly and lamellipodium formation[15] (Supplementary Fig. 14). To test this we used a LOVTRAP construct to acutely release Rac1Q61L and performed spectral analysis (Fig. 3d and Supplementary Fig. 13c). Compared to the Vav2-response, the Rac1-induced oscillations showed a mild frequency density increase between 3 mHz and 4 mHz. The absence of a resonator response could relate to the fact that the activity of RacQ61L cannot be modulated by GTPase-regulatory pathways, which might be essential for the restoring circuitry. Therefore, we repeated these experiments by producing a LOVTRAP-construct for the Rac1-specific GEF Tiam1. Acute release of Tiam1 also had no effect on the spectra (Fig. 3d and Supplementary Fig. 13c). Hence, activation of cells with Vav2 promotes both the stimulation and the restoration required for cyclic protrusion and retraction.

Vav2 interacts with phospholipid products of the phosphoinositide (PI) 3-kinase[15, 16]. These are thought to localize at the protruding cell edge via association of PI3K with focal adhesions[17] and/or via direct or indirect activation of PI3K downstream of Rho-family GTPases[18, 19]. Therefore, we tested whether inhibition of PI3K would abolish the protrusion - retraction resonator. We found no resonance when we irradiated cells expressing LOVTRAP-Vav2 if the medium contained the PI3K inhibitor LY294002 (Fig. 3d and Supplementary Fig. 13c). To further test this model, we used a LOVTRAP-Vav2 construct harboring a point mutation of Vav2’s PH domain that lowers interaction with lipid products[20]. Intriguingly, although optogenetic release of this construct stimulated

protrusion-retraction cycles over a broad range of frequencies, the narrow-band resonance observed with wildtype Vav2 was gone (Fig. 3d and Supplementary Fig. 13c).

LOVTRAP uses the new Zdk reagents in a simple and versatile approach that can be applied to many proteins. Protein release occurs with subsecond kinetics and reversibility can be tuned from <3 to ~500 seconds. The Zdk reagents can be building blocks for other optogenetic tools, providing light-induced dissociation with > 150-fold change in affinity. LOVTRAP's precise and reversible control of activation kinetics was used to explore a signaling circuit that governs cell edge oscillations, revealing a natural resonance frequency and an essential role for Vav2. We anticipate that in a similar manner LOVTRAP can shed light on the host of processes that rely on oscillating cellular signals.

ONLINE METHODS

Z-LIBRARY CONSTRUCTION

The synthetic gene encoding the Z library was assembled by annealing and enzymatically extending primers ZL-U141 and ZL-B143 (Supplementary Table 4, Genelink, NY) that have complementary 3′ ends. Codon NNK (N=G, A, C, T; K=G, T) was used to encode randomized residues. The resulting dsDNA was amplified by PCR using primer ZL-5-66 and ZL-3-57 (Supplementary Table 4). The cycle numbers were optimized to avoid over-amplification by running small scale PCR reactions and checking the product from different cycles on 2% agarose gels. A small portion of the final cDNA library was cloned into pJet1.2 vector (Thermo Scientific) and transformed into NEB5α competent cells. 95 colonies were picked and sequenced to check the codon bias.

mRNA DISPLAY

The C450A and I539E mutants of the LOV2 domain of *Avena sativa* (oat) phototropin1 (404-546) were cloned into the bacterial expression vector pProEx-HTb containing N-terminal His_6-tag followed by an Avi-tag. The proteins were expressed in *E. coli* strain CVB101 (Avidity). They were induced using 0.5 mM isopropyl β-D-1-thiogalactopyranoside (IPTG, sigma) with 100 μM Biotin (Sigma) to express biotinylated LOV2 proteins, or with 0.5 mM IPTG without Biotin to express unbiotinylated LOV2 proteins. The proteins were purified using a HisTrap FF column (GE Healthcare).

The mRNA-protein fusion library was generated and purified according to our published protocol.[21] Reverse transcription was performed to convert the mRNA-protein into cDNA/mRNA-protein form. The purified fusion library was diluted in a binding buffer (50 mM Tris-HCl pH 7.5, 150 mM NaCl, 0.05% Tween-20, 1 mg/mL BSA, 1 mg/mL yeast tRNA and 0.5 mM EDTA) and passed through 75 μL Streptavidin UltraLink Plus Resin (Thermo Scientific) pretreated with 1 mg/mL BSA and 1 mg/mL yeast tRNA to minimize the sequences that nonspecifically bound to streptavidin and/or the matrix. The flowthrough was incubated with LOV2 C450A pre-immobilized on 75 μL streptavidin beads for 90 minutes at room temperature. In rounds 1–5, the beads were washed with 300 μL washing buffer (50 mM Tris-HCl pH 7.5, 150 mM NaCl, 0.05% Tween-20), while in the rounds 6–12, the beads were washed with 300 μL washing buffer containing 5 mg/mL LOV2 I539E to minimize the

enrichment of sequences that bound to the lit form of LOV2, followed by a wash with 300 μL washing buffer. In rounds 1–5, the selected library was eluted by incubating the beads with 150 μL eluting buffer (50 mM Tris-HCl pH 7.5, 150 mM NaCl, 0.05% Tween-20, 1.5 mM $MgCl_2$) contains 1 U RNase H (Thermo Scientific) for 120 minutes at 37°C, while in the rounds 6–12, the selected library was competitively eluted by incubating the beads with 300 μL eluting buffer containing 5 mg/mL LOV2 C450A for 60 minutes at room temperature. The elution was treated with 1 U protease K for 60 minutes at room temperature, followed by phenol/chloroform extraction to remove protein components. The enriched cDNA library was regenerated by PCR using primers ZL-5-66 and ZL-3-57.

After 12 rounds of selection, the enriched DNA library was cloned into the pJet1.2 vector and transformed into DH5α. 120 colonies were picked for sequencing.

RADIOMETRIC BINDING ASSAY

The sequences from the selected library were translated *in vitro* in the presence of ^{35}S-Methonine, followed by purtification using HisPur Cobalt Resin (Thermo Scientific). The purified proteins were incubated with different concentrations of biotinylated LOV2 mutants in 96-well filter plates (Pall) at room temperature for 30 minutes. 20 μL Streptavidin UltraLink Plus Resin was added and the suspension was shaken for 60 minutes. The flowthrough was removed and the beads were washed with 3 bed volumes of washing buffer. 200 μL scintillation liquid was added in each well and the top of the plate was sealed using a transparent sealer. The plate was rotated to mix well, then read using a scintillation plate reader.

BIO-LAYER INTERFEROMETRY (BLI) ASSAY

GST-Zdk1 protein and LOV2 w.t. were expressed and purified as described above. LOV_3, LOV_4 and LOV_5 proteins were gifts from Dr. Brian Kuhlman. The binding kinetics were determined using an Octet QKe system (forteBio). Anti-GST biosensors were equilibrated in an assay buffer (phosphate-buffered saline with 1 mg/ml BSA and 0.05% Tween-20) for 60 seconds, then the tips were loaded with 100 nM GST-Zdk1 for 300 seconds. The association and dissociation of LOV2 proteins were examined by incubating the Zdk-loaded tips with 50, 100, 200 and 500 nM LOV2 proteins for 300 seconds and then in assay buffer for 300 seconds. Kinetics data were analyzed using forteBio software (forteBio). The curves were fit globally using a 1:1 model.

PROTEIN CRYSTALLIZATION

The C450A mutant of the LOV2 domain of *Avena sativa* (oat) phototropin1 (404-546) was cloned into the bacterial expression vector pGEX (GE Healthcare) containing an N-terminal GST-tag and His_6-tag followed by a TEV protease cleavage site. The Zdk1, Zdk2 and Zdk3 proteins were cloned into pQE-80L (Qiagen) containing an N-terminal His_6-tag followed by a TEV protease cleavage site. The proteins were purified using a HisTrap FF column (GE Healthcare).

After elution from the HisTrap FF column using a linear gradient of 10–500 mM imidazole in the same buffer, the proteins were mixed with TEV protease using a 1:20 molar ratio of

TEV:substrate and dialyzed overnight at 4 °C against TEV buffer (50 mM Tris-HCl pH 7.5, 100 mM NaCl, 1 mM dithiotreitol). The dialyzed sample was loaded onto the HisTrap FF column to remove cleaved GST-/His_6-tag and His_6-TEV. The flow-through was concentrated and subjected to gel filtration chromatography on a Superdex 75 column (GE Healthcare) equilibrated with TEV buffer. The eluted protein was concentrated, aliquoted, frozen in liquid nitrogen and stored at −80 °C.

Crystallization was performed at 20 °C in the dark using the vapor-diffusion method. Crystal handling was done under orange light with a 2 mm thick OG570 filter (Schott, Germany) shielding the microscope bulb. To allow complex formation of LOV2(C450A) and Zdk1 both proteins were incubated for 60 min in a 1:1 molar ratio in washing buffer. The complexes of LOV2(C450A) with Zdk2 or Zdk3 were formed by mixing both components in a 1:1 stoichiometry and incubating for 30 min on ice. Crystals of LOV2-Zdk1 were obtained by mixing equal volumes of protein solution (at 10.0 mg/ml) with 2 M $(NH_4)_2SO_4$, 0.1 M sodium citrate pH 3.5 reservoir solution. Tetragonal crystals of the LOV2-Zdk1 complex grew to final dimensions within 1 week. For cryoprotection, crystals were transferred to reservoir solution containing 25% (v/v) glycerol and, after 1-min incubation, crystals were cryocooled in liquid nitrogen. Box-shaped crystals of LOV2-Zdk2 complex were grown by mixing equal volumes of preformed protein complex solution (at 15.7 mg/ml), reservoir solution containing 0.1 M tri-sodium citrate pH 5.6, 0.2 M ammonium acetate, 32% (w/v) PEG 4000 and 0.1 M copper(II) chloride solution as an additive. Before flash-cooling in liquid nitrogen the crystals were briefly washed in cryoprotectant solution consisting of the reservoir solution with PEG 4000 concentration increased to 40% (w/v). Rod-shaped crystals of LOV2-Zdk3 complex were obtained by mixing equal volumes of preformed protein complex solution (at 16.5 mg/ml) and reservoir solution containing 0.1 M citric acid pH 4.0, 1.0 M lithium chloride, 18% (w/v) PEG 6000. Crystals were briefly rinsed in cryoprotectant solution composed of the corresponding reservoir solution supplemented with 20% (v/v) glycerol prior to flash-cooling in liquid nitrogen.

X-RAY DIFFRACTION DATA COLLECTION AND STRUCTURE DETERMINATION

Single crystal X-ray diffraction data were collected at 100 K on the X10SA beamline at the Swiss Light Source (Paul Scherrer Institute, Villigen, Switzerland). The data were processed with XDS.[22] All three structure of LOV2-Zdk complexes were determined by molecular replacement using Phaser[23]. The structure of LOV2-Zdk1 was determined with individual search models of LOV2 (PDB entry 2V0U) and protein Z (PDB entry 1LP1, chain A). A unique solution was obtained for one molecule each in the asymmetric unit. However, initial density maps suggested the presence of another protein Zdk1 molecule with altered N-terminal helix conformation that was manually added during the initial rounds of refinement. The structure of LOV2-Zdk2 complex was determined using LOV2 domain coordinates from PDB entry 2WKQ and a homology model of Zdk2 (residues 9-58) generated with SWISS-MODEL[24] based on PDB entry 2KZJ as a search models. The structure of LOV2-Zdk3 complex was determined using the same LOV2 coordinates and a homology model of Zdk3 (residues 9-58) based on PDB entry 1Q2N. The final models were optimized in iterative cycles of manual rebuilding using Coot[25] and refinement using phenix.refine[26].

Data collection and refinement statistics are summarized in Supplementary Table 5. Model quality was validated using validation methods implemented in PHENIX[27].

PLASMID CONSTRUCTION AND TRANSFECTION

All plasmids were generated by overlap PCR and subcloned into mammalian expression vector pTriEx by restriction enzyme digestion and ligation. The plasmids (Supplementary Table 6) were co-transfected into the cells using FuGene 6 (Promega), following the manufacturer's instructions.

CELL LINES

All cell lines were obtained from the American Type Culture Collection (ATCC, Manassas, Virginia) and were tested for mycoplasma by the UNC Tissue Culture Core Facility. No cells on the ICLAC list of commonly misidentified cells were used in this work.

WESTERN BLOTTING

HeLa cells were transiently co-transfected with LOVTRAP plasmids for 20 hours before lysis in RIPA buffer. The cell extracts were adjusted to the same amount of total cellular protein (50 μg), and electrophoresed in a 4% to 15% gradient polyacrylamide gel. After electrophoretic transfer to a PVDF membrane at 1.0A for 30 min, the membranes were blocked with TBST (10mM Tris-HCl, pH7.5, 150mM NaCl, 0.05%Tween-20) containing 5% BSA for 1 hour at room temperature. The primary antibodies (mouse monoclonal anti-Rac1 antibody from Cytoskeleton, Inc., Cat. # ARC03, 1:500 dilution[28]; mouse monoclonal anti-GFP Antibody from Clontech, Cat# 632381, 1:1000 dilution[29]; and mouse monoclone anti-human vinculin antibody Clone h-VIN1 from Sigma, Cat# V9131, 1:200 dilution[30]) in TBST were placed on the membrane and incubated at 4°C overnight. After three washings with TBST over 5 min, the second antibody (Anti-mouse IGG, conjugated with DyLight680, from Cell Signaling, Cat#5470P, 1:10,000 dilution[31]) was applied. After three washings with TBST over 5 min, the membrane was scaned by the Odyssey® Infrared Imaging System (LI-COR Biosciences, Lincoln, NE).

FLOW CYTOMETRY

HeLa cells were transiently co-transfected with LOVTRAP plasmids for 20 hours, then rinsed, trypsinized, washed and resuspended in fresh DPBS buffer at a density of 106 cells/ml. 5 μM DilC1(5) or MitoSOX Red were added to the cells, and the cells were then incubated at 37°C for 30min according to Mukhopadhyay et al[32]. Samples were analyzed using an LSR II flow cytometer (BD Biosciences) at the UNC Flow Cytometry Core Facility. The gate was set so that only cells labeled with dyes were displayed.

LIVE CELL IMAGING

HeLa cells were transiently co-transfected with LOVTRAP plasmids 20 – 28 hours before imaging. Cells used for live cell imaging were seeded on coverslips coated with 10 mg/ml fibronectin in Ham's F-12K medium free of Phenol Red and containing 0.5% FBS. Coverslips were mounted in an Attofluor live cell chamber (Invitrogen) and placed on a heated microscope stage (Warner). Images were acquired using an Olympus IX81-ZDC

microscope equipped with a CoolSNAP HQ2 14-bit camera (Photometrics). Bandpass and neutral density filters (Chroma) were switched using motorized filter wheels (Ludl Electronic Products) controlled by Metamorph Software version 7.6.4. YFP and mCherry images were acquired using a 100 W Hg arc lamp with a 1% ND filter and a 510–520 nm or 565–595 nm band-pass filter respectively, for 500 ms. For photoactivation, a 5% ND filter and a 426–446 nm band-pass filter were used. Unless otherwise indicated, activation was carried out using a pulse protocol alternating 5 seconds light with 5 seconds dark. This minimizes photodamage while maintaining greater than 80% activity for wild type LOV2. Images were processed post acquisition via shading correction, background subtraction, and binary masking using Metamorph software (Molecular Devices).

BLIND SCORING

Images from VAV2 or RhoA activation were mixed with images from control cells and a naïve observer was asked to score the cells, stating whether the blue light induced or reduced ruffling.

IMAGE ANALYSIS

Cell outlines were identified using intensity based thresholding on all frames of time lapse movies (Movie 8). The cell edge was subsequently divided into 1μm segments, or windows, where the average normal velocity vector was calculated by tracking these segments from one frame to the next. A velocity profile for each window was built using the signed normal vector magnitude of the respective window. The cell edge velocity map (as shown in the main text, figure 3a) was constructed by stacking up the velocity profiles from all windows, as described in Vilela et al., 2013[33].

EDGE VELOCITY FREQUENCY ANALYSIS

A signal processing technique known as Hilbert-Huang transform was used to analyze the time-frequency content of the edge velocity profiles over time [14]. In a first step this technique applies the empirical mode decomposition algorithm (EMD) to decompose the signal into monochromatic components (components with only one frequency at each time point). Supplementary Fig. 13 shows an example, in which a test signal is decomposed into eight empirical modes. Subsequently, each mode is Hilbert transformed and used to build a mathematical construct referred to as a Hilbert Spectrum. Two important features were inferred from the spectrum at all time points of a time series: the instantaneous frequency spectrum defined by the combination of frequencies of the monochromatic modes and their respective amplitudes. The final time series spectrum was obtained by arranging instantaneous frequencies and amplitudes over time for all decomposed components, as shown in Supplementary Fig. 13 box.

Each signal extracted from a window of a given cell gave rise to one time-frequency spectrum. The spectrum for a given cell was then obtained by bootstrapping the mean amplitude for each time-frequency pair of all windows[34] (Supplementary Fig. 13 flowchart). The same bootstrapping procedure was applied to obtain a final spectrum extracted from several cells. To allow combination of cells with different ranges of protrusion/retraction

velocity each individual cell spectrum was first normalized. A specific bootstrap technique for frequency domain data was used to avoid bias from dominant cells or cell windows [14].

CODE AVAILABILITY

Software codes developed for cell protrusion tracking and spectral analysis will be made available through the Danuser lab website. In particular, the protrusion tracking methods are included in a larger package for the analysis of cell signaling dynamics that is currently in revision for a separate publication.

Supplementary Material

Refer to Web version on PubMed Central for supplementary material.

Acknowledgments

This work was funded by the NIH grants R01-GM090317 (K.M.H. and G.D.), P01-GM103723 (K.M.H. and G.D.), R01-DA036877 (K.M.H.), R01-CA157738 (R.L.), and by the Max Planck Society, German Research Foundation DFG, FOR 1279 (I.S.). HW is a recipient of an Arthritis Foundation Postdoctoral Fellowship. We thank Elisabeth Hartmann for crystallizing Zdk-LOV complexes, Ryan Littlefield for providing LOV2 peptides, and Evan Trudeau for cloning help. Diffraction data were collected at the Swiss Light Source, beamline X10SA, of the Paul Scherrer Institute, Villigen, Switzerland. We thank the Heidelberg data collection team and the PXII staff for their support in setting up the beamline and Chris Roome for expert support of the crystallographic software. The UNC Flow Cytometry Core Facility is supported in part by P30 CA016086 Cancer Center Core Support Grant to the UNC Lineberger Comprehensive Cancer Center.

References

1. Weitzman M, Hahn KM. Optogenetic approaches to cell migration and beyond. Curr Opin Cell Biol. 2014; 30:112–120. [PubMed: 25216352]
2. Nord K, et al. Binding proteins selected from combinatorial libraries of an alpha-helical bacterial receptor domain. Nat Biotechnol. 1997; 15(8):772–7. [PubMed: 9255793]
3. Kay CW, et al. Blue light perception in plants. Detection and characterization of a light-induced neutral flavin radical in a C450A mutant of phototropin. J Biol Chem. 2003; 278(13):10973–82. [PubMed: 12525505]
4. Harper SM, Christie JM, Gardner KH. Disruption of the LOV-Jalpha helix interaction activates phototropin kinase activity. Biochemistry. 2004; 43(51):16184–92. [PubMed: 15610012]
5. Harper SM, Neil LC, Gardner KH. Structural basis of a phototropin light switch. Science. 2003; 301(5639):1541–4. [PubMed: 12970567]
6. Kanaji S, et al. Characterization of the signal that directs Tom20 to the mitochondrial outer membrane. J Cell Biol. 2000; 151(2):277–88. [PubMed: 11038175]
7. Zoltowski BD, Vaccaro B, Crane BR. Mechanism-based tuning of a LOV domain photoreceptor. Nat Chem Biol. 2009; 5(11):827–34. [PubMed: 19718042]
8. Kawano F, et al. Fluorescence imaging-based high-throughput screening of fast- and slow-cycling LOV proteins. PLoS One. 2013; 8(12):e82693. [PubMed: 24367542]
9. Levskaya A, et al. Spatiotemporal control of cell signalling using a light-switchable protein interaction. Nature. 2009; 461(7266):997–1001. [PubMed: 19749742]
10. Krause M, Gautreau A. Steering cell migration: lamellipodium dynamics and the regulation of directional persistence. Nat Rev Mol Cell Biol. 2014; 15(9):577–90. [PubMed: 25145849]
11. Vicente-Manzanares M, Webb DJ, Horwitz AR. Cell migration at a glance. J Cell Sci. 2005; 118(Pt 21):4917–9. [PubMed: 16254237]
12. Machacek M, Danuser G. Morphodynamic profiling of protrusion phenotypes. Biophys J. 2006; 90(4):1439–52. [PubMed: 16326902]

13. Abe K, et al. Vav2 is an activator of Cdc42, Rac1, and RhoA. J Biol Chem. 2000; 275(14):10141–9. [PubMed: 10744696]
14. Huang, NE.; Shen, SS. Interdisciplinary Mathematical Sciences. 2. Hackensack New Jersey: World Scientific; 2014. Hilbert-Huang transform and its applications; p. xiip. 386
15. Hornstein I, Alcover A, Katzav S. Vav proteins, masters of the world of cytoskeleton organization. Cell Signal. 2004; 16(1):1–11. [PubMed: 14607270]
16. Han J, et al. Role of substrates and products of PI 3-kinase in regulating activation of Rac-related guanosine triphosphatases by Vav. Science. 1998; 279(5350):558–60. [PubMed: 9438848]
17. Chen HC, Guan JL. Association of focal adhesion kinase with its potential substrate phosphatidylinositol 3-kinase. Proc Natl Acad Sci U S A. 1994; 91(21):10148–52. [PubMed: 7937853]
18. Weiner OD, et al. A PtdInsP(3)- and Rho GTPase-mediated positive feedback loop regulates neutrophil polarity. Nat Cell Biol. 2002; 4(7):509–13. [PubMed: 12080346]
19. Yang HW, et al. Cooperative activation of PI3K by Ras and Rho family small GTPases. Mol Cell. 2012; 47(2):281–90. [PubMed: 22683270]
20. Booden MA, Campbell SL, Der CJ. Critical but distinct roles for the pleckstrin homology and cysteine-rich domains as positive modulators of Vav2 signaling and transformation. Mol Cell Biol. 2002; 22(8):2487–97. [PubMed: 11909943]
21. Cotton SW, et al. Selection of proteins with desired properties from natural proteome libraries using mRNA display. Nat Protoc. 2011; 6(8):1163–82. [PubMed: 21799486]
22. Kabsch W, Xds. Acta Crystallogr D Biol Crystallogr. 2010; 66(Pt 2):125–32. [PubMed: 20124692]
23. McCoy AJ, et al. Phaser crystallographic software. J Appl Crystallogr. 2007; 40(Pt 4):658–674. [PubMed: 19461840]
24. Arnold K, et al. The SWISS-MODEL workspace: a web-based environment for protein structure homology modelling. Bioinformatics. 2006; 22(2):195–201. [PubMed: 16301204]
25. Emsley P, et al. Features and development of Coot. Acta Crystallogr D Biol Crystallogr. 2010; 66(Pt 4):486–501. [PubMed: 20383002]
26. Afonine PV, et al. Towards automated crystallographic structure refinement with phenix.refine. Acta Cryst. 2012; D68(Pt 4):352–67.
27. Adams PD, et al. PHENIX: a comprehensive Python-based system for macromolecular structure solution. Acta Crystallogr D Biol Crystallogr. 2010; 66(Pt 2):213–21. [PubMed: 20124702]
28. Seidelin JB, et al. Cellular inhibitor of apoptosis protein 2 controls human colonic epithelial restitution, migration, and Rac1 activation. Am J Physiol Gastrointest Liver Physiol. 2015; 308(2):G29–9.
29. Lorenz H, Hailey DW, Lippincott-Schwartz. Fluorescence protease protection of GFP chimeras to reveal protein topology and subcellular localization. J Nature Methods. 2006; 3:205–210.
30. Risse P, et al. Interleukin-13 inhibits proliferation and enhances contractility of human airway smooth muscle cells without change in contractile phenotype. American Journal of Physiology - Lung Cellular and Molecular Physiology. 2011 Jun 01.
31. Jia L, et al. Defining pathways of spindle checkpoint silencing: functional redundancy between Cdc20 ubiquitination and p31(comet). Mol Biol Cell. 2011 Nov; 22(22):4227–35. [PubMed: 21937719]
32. Mukhopadhyay P, et al. Simultaneous detection of apoptosis and mitochondrial superoxide production in live cells by flow cytometry and confocal microscopy. Nat Protoc. 2007; 2(9):2295–301. [PubMed: 17853886]
33. Vilela M, et al. Fluctuation analysis of activity biosensor images for the study of information flow in signaling pathways. Methods Enzymol. 2013; 519:253–76. [PubMed: 23280114]
34. Zoubir, AM.; Iskander, DR. Bootstrap Techniques for Signal Processing. Cambridge, England; New York: Cambridge; 2004. p. xivp. 217

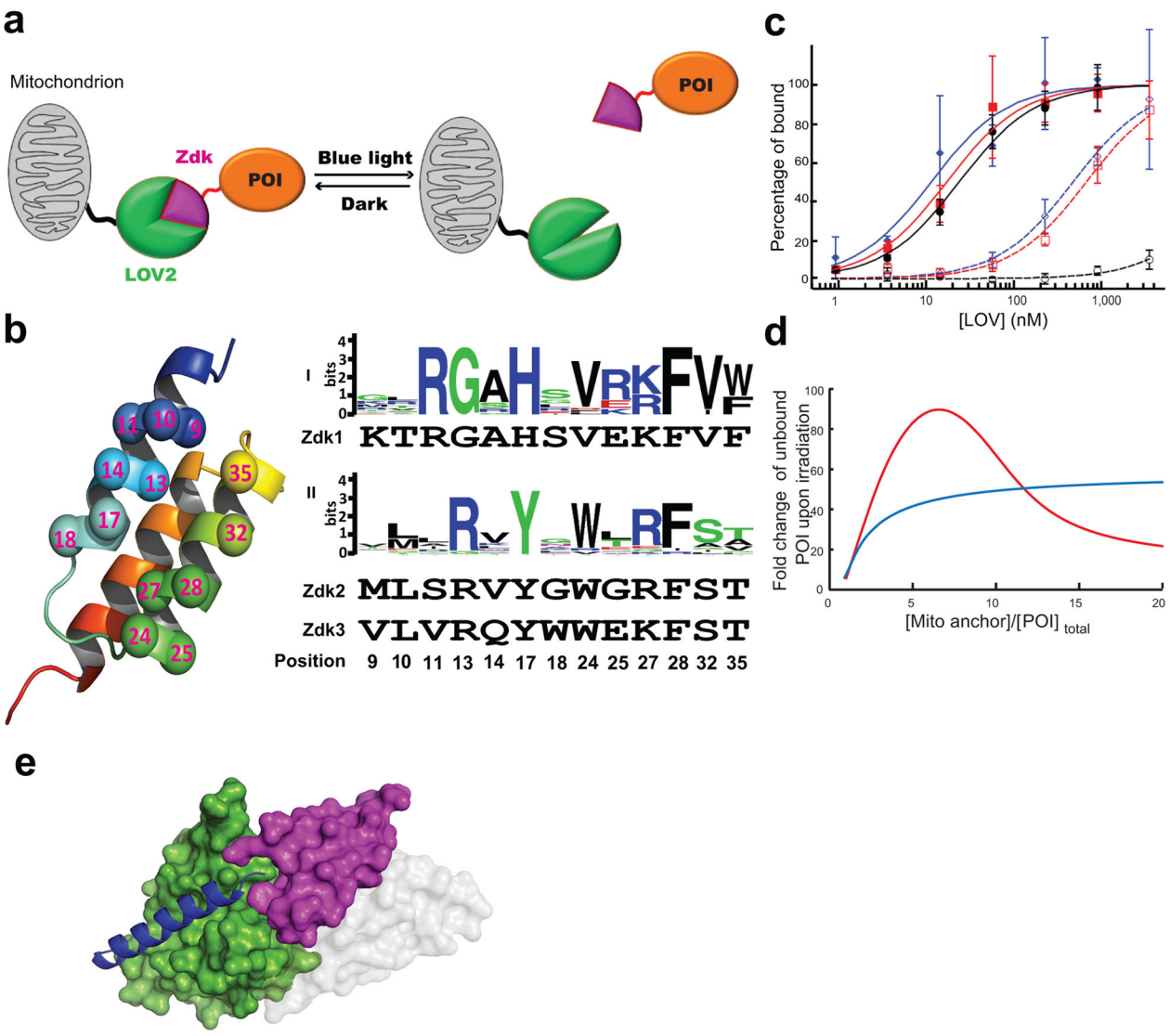

Figure 1. Generation of Zdk and design of LOVTRAP

(**a**) LOV2 is anchored to the mitochondrial outer membrane. The protein of interest (POI) is attached to Zdk, a reagent that binds selectively to the dark state of LOV2. The POI is sequestered at mitochondria in the dark and released when cells are irradiated. (**b**) Thirteen residues along the first and second helices of the Z domain from protein A were randomized to generate a variable surface (left). Two consensus sequences bound specifically to the dark state of LOV2 (right). (**c**) Binding of Zdk isoforms to LOV2's dark state (C450A mutant) versus lit state (I539E mutant) (n=4 for each curve). Dark versus lit affinities of Zdk1 (black), Zdk2 (red) and Zdk3 (blue) were 26.2±2.2 nM/>4 μM, 17.0±3.9 nM/761±78 nM, and 11.4±3.6 nM/537±37 nM, respectively. Error bars are the s.d. of replicates. (**d**) The amount of protein released upon irradiation depends upon the relative expression levels of the mitochondrial anchor and the POI. This model shows the effects of using Zdk1 on the POI and LOV2 at the mitochondria (red), or vice-versa (blue). Optimal response is seen when the protein attached to the mitochondria is in 4–10 fold excess over the POI. LOV2 on

the mitochondria produces less free POI in the dark, and Zdk on mitochondria leads to more complete release. (**e**) Crystal structure of the LOV2-Zdk1 complex. Zdk1 (magenta) docks on the core domain of LOV2 (green) and the C-terminal residues of the LOV2 Jα helix (blue).

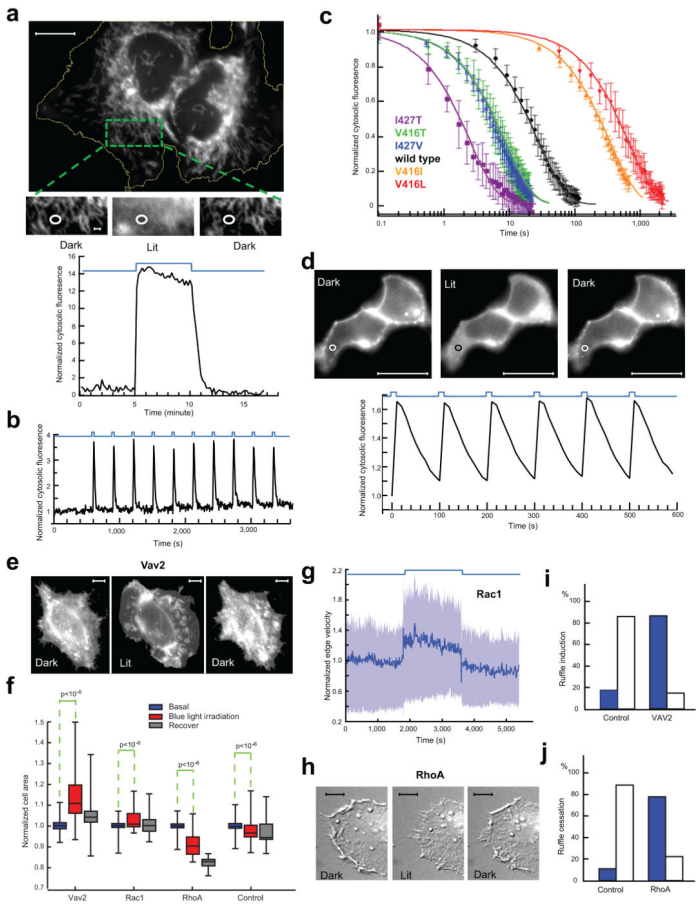

Figure 2. Protein control by LOVTRAP

(**a**) Zdk1 was attached to the outer membrane of mitochondria and mCherry was attached to LOV2. Monitoring fluorescence intensity at a spot away from mitochondria (circle) revealed release and return kinetics (blue = irradiation). (**b**) Repeated irradiation cycles. (**c**) Effects of LOV2 mutants on return $t_{1/2}$: I427T (purple, n=18) 1.7±0.6; V416T (green, n=12) 5.0±2.0; I427V (blue, n=15): 5.5±0.8; wild type (black, n=12) 18.5±3.7; V416I (orange, n=3) 239±5; V416L (red, n=6) 496±38. (**d**) HEK293 cells with LOV2 attached to the plasma membrane and Zdk attached to mCherry. Fluorescence monitored as in (**a**). (**e**) Reversible cell protrusion produced by light-induced release of constitutively active Vav2. (**f**) Cell area before, during and after light-induced release of constitutively active Vav2 (7 cells), Rac1 (7 cells), RhoA (4 cells) and Control (5 cells). Wilcoxon rank test and permutation test were performed to the medians before and during irradiation. For both, $p < 1e\text{-}6$. (**g**) Light-induced release of constitutively active Rac1 reversibly increases velocity. Dark blue line indicates median, band indicates 95% confidence interval, n=2017 edge locations from m = 7 cells. (**h**) Release of constitutively active RhoA led to irreversible contraction and reversible decrease in ruffling. (**i**) Quantitation of Vav2 effects on ruffling. White = percent cells in which ruffling was induced, blue = percent cells with no obvious effect on ruffling. Cells were transfected either with LOVTRAP (Vav2, n=14) or with LOV and Zdk1 only (Control, n=18). (**j**) Inhibition of ruffling by RhoA(Q63L), graphed as in i. Control =

expression of LOV2 and Zdk1 only (n= 9), RhoA = LOVTRAP (n= 18). All scale bars 10μm except 1(**a**) lower = 1μm.

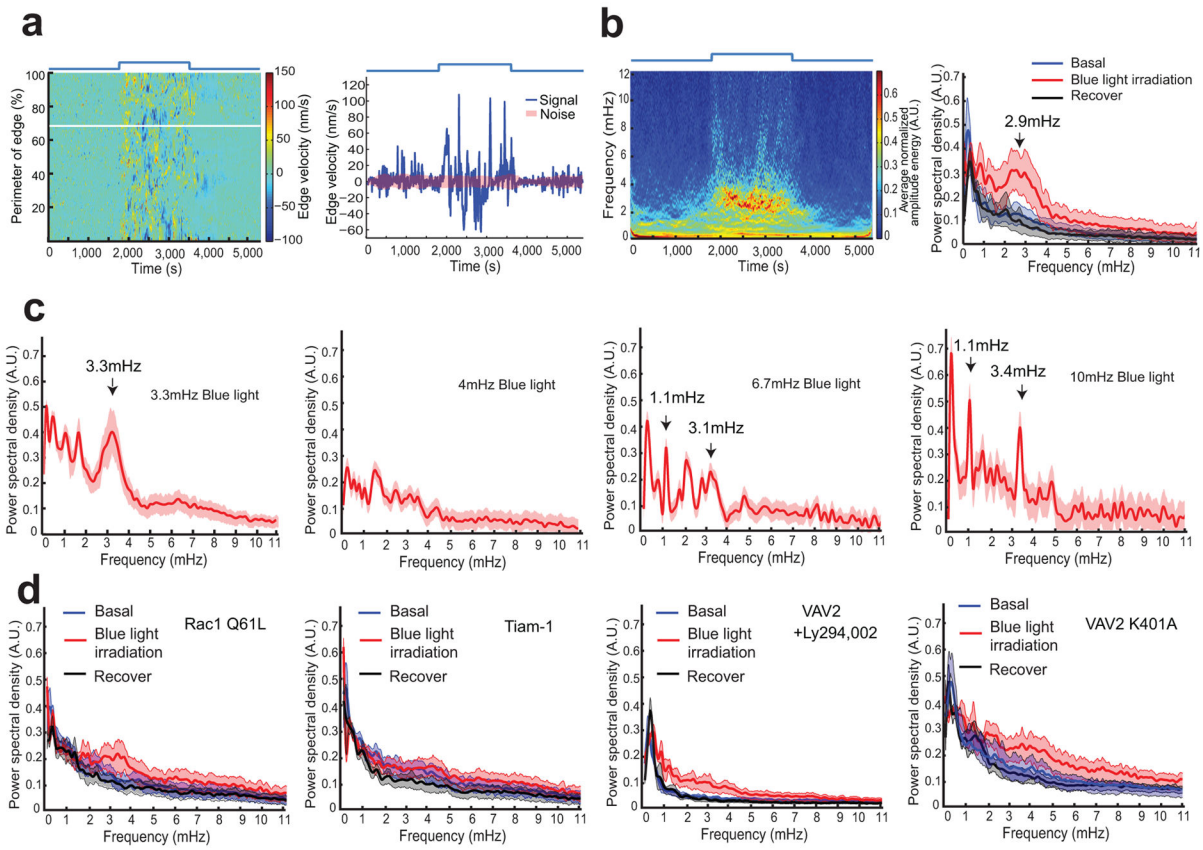

Figure 3. Resonance in HeLa cell protrusion-retraction cycles upon acute release of Vav2

(**a**) Kymograph of cell edge velocity (y-axis, distance along cell perimeter; x-axis, time) (left panel). Time series of instantaneous edge velocity sampled at one cell edge location (right panel), indicated in the left panel by a white horizontal line. Red area, noise band as determined by empirical mode decomposition of the time series (see Methods). Blue lines at the top of each panel show the timing and duration of irradiation. (**b**) Left, representative spectrogram of HeLa cell protrusion cycles in response to Vav2 release (blue line indicates irradiation). Right, power density as a function of the temporal frequency of cell edge protrusion-retraction cycles, separated into before (blue), during (red), and after (gray) release of Vav2. Center line indicates median density, band indicates 95% confidence interval about median, calculated from n=2606 edge locations sampled in m=7 cells. (**c**) Power densities from cells stimulated with 3.3mHz, 4mHz, 6.7mHz and 10mHz blue light pulses. Center line and confidence bands as in B. (for each panel, n = 2044 edge locations sampled in m = 6 cells). (**d**) Changing power densities during acute stimulation of constitutively active Rac1Q61L (n=357 edge locations, m=2 cells), endogenous Rac1 via release of TIAM-1 DH/PH domain (n=1546 edge locations, m=4 cells), constitutively active Vav2 in the presence of the PI3K inhibitor LY294,002 (n=2350 edge location, m=7 cells), and Vav2 K401A mutant with impaired binding to PI3K-generetaed phospholipid products (n=1439 edge locations, m=4 cells).